Composites Part B 91 (2016) 56–64

Contents lists available at ScienceDirect

Composites Part B

journal homepage: www.elsevier.com/locate/compositesb

Strong viscous behavior discovered in nanotube mats, as observed in boron nitride nanotube mats

Xinghua Hong [1], Daojun Wang, D.D.L. Chung[*, 2]

Composite Materials Research Laboratory, University at Buffalo, State University of New York, Buffalo, NY 14260-4400, USA

ARTICLE INFO

Article history:
Received 18 July 2015
Received in revised form
23 October 2015
Accepted 1 January 2016
Available online 8 February 2016

Keywords:
A. Ceramic fiber
A: Nano-structures
B: Vibration
B: Rheological properties

ABSTRACT

Strong viscous behavior has been discovered in nanotube mats, as observed in boron nitride nanotube (BNNT) mats under low-amplitude dynamic flexure. The solid part of the mat (BNNTs) exhibits strong viscous character (loss tangent up to 13), strong elastic character (storage modulus up to 2.3 GPa), and strong mechanical energy dissipation ability (loss modulus up to 7.3 GPa), indicating exceptional vibration damping ability. The loss tangent of the solid part of the mat decreases with increasing solid content, while the storage and loss moduli of the solid part increases, due to the increasing difficulty for frictional sliding among the BNNTs.

1. Introduction

Nanotubes are commonly used in the form of mats or yarns. A mat or yarn consists of a number of nanotubes that are weakly held together by van der Waals forces. There is no matrix material, so that a mat or yarn includes a substantial proportion of air voids. However, a small amount of binder may be present to hold the nanotubes together at their junctions.

A yarn is a filament in which the nanotubes have preferred orientation along the filament axis. A mat is a sheet in which the nanotubes most commonly have preferred orientation in the plane of the sheet. However, it is also possible for a mat to exhibit preferred orientation of the nanotubes in the direction perpendicular to the plane of the sheet, as in the case of vertically aligned nanotube arrays.

Due to the weak linkage between the nanotubes in a mat or yarn, the strength and elastic modulus of a mat [1] or yarn [2,3] are much lower than those of a single nanotube, as shown for the case of carbon nanotubes. The weak inter-nanotube linkage suggests ease of sliding between adjacent nanotubes in a mat or yarn [1]. The sliding in turn suggests the presence of viscous character. Indeed, a minor degree of viscous character is suggested by a low degree of stress relaxation observed in carbon nanotube mats, though the viscoelastic properties have not been determined from the stress relaxation results [1].

Viscous behavior is necessary for vibration damping and mechanical isolation. Damping refers to the reduction of the vibration amplitude by the conversion of the mechanical energy to another form of energy, typically thermal energy. This energy conversion is known as mechanical energy dissipation. Mechanical isolation refers to the avoiding of the propagation of mechanical energy from one object to another, typically achieved through the spreading of the mechanical energy along an isolation material positioned between the two objects. Mechanical vibrations can affect the performance, durability and safety of structures, whether they occur during normal structural operation or extreme events (such as earthquakes).

Rubber and other elastomers are highly effective for mechanical isolation, due to their resiliency and consequent cushioning effect. However, they are not effective for damping, due to their softness. Furthermore, rubber suffers from their tendency to degrade and lose its elastomeric character in the environment, particularly upon exposure to ultra-violet radiation. In addition, rubber is poor in the ability to withstand elevated temperatures or chemically harsh environments.

For effective vibration damping, materials that are both stiff and capable of mechanical energy loss are needed. In other words, strong viscous character and strong elastic character are both

* Corresponding author. Tel.: +1 716 645 3977.
E-mail address: ddlchung@buffalo.edu (D.D.L. Chung).
[1] Permanent address: Key Laboratory of Textile Science & Technology, College of Textile, Donghua University, Shanghai 201620, China.
[2] http://alum.mit.edu/www/ddlchung.

http://dx.doi.org/10.1016/j.compositesb.2016.01.001
1359-8368/

needed. A collection of nanotubes, whether the collection is in the form of a mat or a yarn, may possibly be attractive in this regard. This is because the stiffness is expected to stem from the inherently high elastic modulus of the nanotubes and the mechanical energy loss ability is expected to stem from the movement between the nanotubes in the mat or yarn. This possibility provides a motivation for this work, which is mainly aimed at studying the viscoelastic behavior of nanotube mats.

The ease of movement between the nanotubes in a mat or yarn is expected to be related to how much the adjacent nanotubes are squeezed (compacted) together. The greater is the squeezing, the closer are the nanotubes to one another, and the less easy is expected of the movement. This notion is supported by the observation that the stress relaxation in carbon nanotube mats decreases with increasing strain under compression [1]. However, the viscoelastic properties and their dependence on the strain have not been obtained from the stress relaxation results [1]. Therefore, this work is also aimed at studying the effect of the extent of squeezing or compaction on the viscoelastic properties.

The viscoelastic character of polymer-matrix composites containing yarns has been reported [3–5]. The viscoelastic behavior of such a composite tends to be dominated by that of the polymer matrix. Furthermore, the presence of the matrix hinders the sliding between the adjacent nanotubes in the composite. Therefore, this paper addresses the viscoelastic behavior of a collection of nanotubes in the absence of a matrix material.

Prior work on nanotube mats emphasizes non-structural properties and non-structural applications. For example, prior work, which is on carbon nanotube mats only, has addressed the electrical conduction behavior [6,7], field emission behavior [8], electrochemical behavior [9–12], optical behavior [7,13], magnetic behavior [14,15], thermal behavior [16,17], chemical sensors [18,19], fluid flow sensors [20], transistors [21,22] and interconnects [23].

The approach used in this work involves dynamic mechanical testing at a controlled frequency [24]. In this forced resonance method, a sinusoidal stress wave with specified values of the static stress and the dynamic stress is imposed on the specimen by using a load cell, and the resulting strain wave (along with the associated static strain and deformation amplitude) is measured by using a displacement transducer. The phase difference δ between the input stress wave and the output strain wave is measured, thereby giving the loss tangent ($\tan\delta$), which describes the degree of viscous character. The ratio of the dynamic stress to the dynamic strain gives the storage modulus, which describes the elastic character and corresponds to the real part of the complex modulus. The imaginary part of the complex modulus is the loss modulus.

This paper uses boron nitride nanotubes (BNNTs) to study the viscoelastic properties of nanotube mats. The BNNT is a structural analogue of the carbon nanotube (CNT), with the carbon atoms in the CNT fully substituted by boron and nitrogen atoms in the BNNT. However, in contrast to the CNT, the BNNT is electrically insulating. Moreover, the BNNT exhibits superior chemical stability. The general notions in the findings of this work regarding BNNT mats are relevant to the mats of other materials, such as CNTs. Furthermore, the general notions in the findings of this work on mats are relevant to yarns, since both mats and yarns involve multiple nanotubes that are in close proximity to one another.

The BNNTs have received considerable recent attention due to their high thermal conductivity, low dielectric constant and high modulus of elasticity [25,26]. Carbon nanotubes (CNTs) exhibit even higher thermal conductivity and modulus of elasticity. The main difference between BNNTs and CNTs is that BNNTs are electrically nonconductive, whereas CNTs are electrically conductive. The combination of low electrical conductivity and high thermal conductivity is not common among materials; diamond is the primary example of a material that exhibits this combination of properties. This combination of properties is valuable for heat dissipation from microelectronic packages, which commonly suffer from overheating. For example, printed circuit boards are preferably made of materials that are electrically nonconductive, such as glass fiber polymer-matrix composites, and the enhancement of the thermal conductivity without increasing the electrical conductivity is desirable.

The objectives of this paper are (i) to study the viscoelastic behavior of nanotube mats, as represented by BNNT mats, (ii) to determine the viscoelastic properties (loss tangent, loss modulus and storage modulus) of a collection of multiple nanotubes in the absence of a binder for the first time, and (iii) to investigate the effect of the extent of proximity between adjacent nanotubes on the viscoelastic behavior of a nanotube mat.

2. Experimental methods

A specimen used in this work is a nanotube mat obtained by the unidirectional compaction of a collection of BNNTs with a very low bulk density in the absence of a binder. The resulting mat is in the plane perpendicular to the direction of pressure application. Due to the large degree of consolidation (i.e., the large decrease in the bulk volume) during compaction, the mat exhibits preferred orientation of the nanotubes in the plane of the mat. For testing under flexure (three-point bending), the specimen is in the shape of a beam with the mechanically neutral plane of the beam in the middle plane perpendicular to the compaction direction.

Based on the measured density of the mat, the solid volume fraction is determined. The solid volume fraction is systematically varied by varying the pressure used in compacting the collection of nanotubes. The higher is the fabrication pressure, the greater is the solid volume fraction. The viscoelastic properties of the solid part of the mat (i.e., the mat with the air contribution excluded) are obtained from the measured viscoelastic properties of the mat by dividing the measured mat property by the solid volume fraction of the mat. This approach is based on the notion that air contributes negligibly to both the elastic and viscous properties. The quantities divided by the solid volume fraction can be considered as the normalized quantities that are independent of the solid volume fraction unless the corresponding property of the solid part changes with the solid volume fraction.

2.1. Materials

The BNNT material is provided by BNNT, LLC (Newport News, VA). The tubes are synthesized using the high temperature/high pressure (HTP) method, also called the pressurized vapor/condenser (PVC) method. This method produces highly flexible, high aspect ratio BNNTs with high crystallinity. According to the manufacturer, the number of walls in a nanotube typically ranges from 1 to 5, with 2 and 3 being the most common; the tube length is up to 200 μm; the specific surface area is up to 300 m^2/g; there are up to 5 BNNTs across each BNNT bundle; the purity is up to 40–50 wt.%, with the impurities in the form of hexagonal BN flakes and elemental boron microdroplets. The as-grown material has a cotton-like appearance, with an unusually low tapped (bulk) density of about 0.25 mg/cm^3. The true density is 1.38 ± 0.12 g/cm^3, though this value is likely an underestimate due to the method of density determination [27]. The energy band gap is 5.7 eV, according to the manufacturer.

The BNNTs are compressed in a cylindrical steel mold (30 mm inner diameter, with a matched steel piston) at pressures ranging from 0.47 to 22.97 MPa. No binder is used. Scanning electron microscope (SEM) images of the BNNT impacts (as viewed from the

top of the mat) are shown in Fig. 1 for the lowest and highest pressures.

The BNNTs show preferred orientation in the plane of the mat, such that the degree of preferred orientation is greater for the higher pressure. This is supported by Fig. 1, which shows that the BNNTs are preferentially in the plane of the photo. Due to the sheet geometry, the unidirectional compaction method of formation of the mat and the high degree of consolidation (volume decrease) during mat fabrication, the presence of preferred orientation is expected. In fact, preferred orientation of fibers or nanotubes in the plane of a fibrous mat is well-known for mats that are made by using either unidirectional compaction [28] or the dispersion-based papermaking method [29]. Both Ref. 28 and 29 pertain to CNTs and clearly show preferred orientation of the CNTs in the plane of the mat (i.e., the plane of the SEM photos).

Fig. 1 shows that the particulate matter is present here and there on the surface of the BNNTs, such that it is not continuous. In spite of the particulate matter, the structure is vastly dominated by the nanotubes. The flexural properties of a mat are governed by the continuous constituent in the mat, namely the BNNT network. However, the discontinuous particulate matter may interfere with the movement of the nanotubes relative to one another. In spite of the possible interference, the movement is easy enough to enable strong viscous behavior that has been observed in the mat (Sec. 3.1).

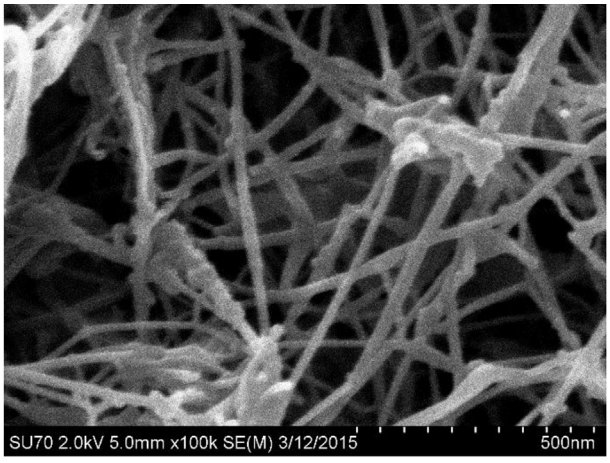

Fig. 1. SEM photographs of BNNT compacts obtained at different fabrication pressures. Each compact is viewed from the top of the mat. (a) The lowest pressure of 0.47 MPa. (b) The highest pressure of 22.97 MPa.

As expected, the BNNTs are more tightly packed for the compact obtained at the higher pressure. After compaction, the resulting disc is cut manually using scissors along three parallel lines at and near to a diameter to obtain two beams that are symmetrically on the two sides of the diameter. The higher is the compaction pressure, the greater are both the density (ranging from 0.11 to 0.51 g/cm^3) and the solid content (ranging from 8 to 37 vol.%) of the mat. The density is determined by measurement of the mass and volume of each beam. The solid content (vol.%) is obtained by dividing the measured density of the mat by the true density of the BNNT. The dimensions, density and solid content of the beams obtained at various compaction pressures are listed in Table 1. Due to the large amount of consolidation during compaction, the BNNTs have preferred orientation in the plane of the beam. However, the orientations of the BNNTs are random in the plane of the beam.

2.2. Testing methods

2.2.1. Dynamic mechanical testing

The method of dynamic mechanical testing is the same as in prior work involving exfoliated graphite compacts [30]. The specimen configuration for dynamic mechanical testing under flexure (three-point bending) is illustrated in Fig. 2. The specimen is a beam, with a span of 20 mm. The measurement time is 5 min for each specimen. At least two specimens of each density are tested and each specimen is tested twice.

Dynamic testing (ASTM D 4065-94) using a sinusoidal stress wave at a controlled low frequency of 0.2 Hz is conducted at room temperature using a dynamic mechanical analyzer (DMA7, Perkin Elmer Corp., Shelton, CT). This low frequency is far away from any vibration resonance frequency of the specimen. In addition, low frequencies are relevant to large structures and there is considerable previously reported comparative data on various materials at

Table 1
The dimensions, density and solid content of BNNT mats obtained by compaction of. BNNTs at various pressures.

Pressure (MPa)	Length (mm)	Width (mm)	Thickness (mm)	Density (g/cm^3)	Solid content (vol.%)
0.47	26.29	7.88	0.706	0.111 ± 0.001	8.04 ± 0.67
0.94	26.38	7.89	0.539	0.145 ± 0.001	10.49 ± 0.87
1.40	26.49	7.91	0.455	0.170 ± 0.001	12.34 ± 1.03
2.32	26.54	7.96	0.385	0.200 ± 0.001	14.46 ± 1.21
4.71	26.58	7.99	0.275	0.278 ± 0.001	20.14 ± 1.71
9.38	26.63	8.01	0.207	0.368 ± 0.002	26.64 ± 2.29
13.70	26.77	8.01	0.190	0.390 ± 0.003	28.27 ± 2.44
18.58	26.85	8.02	0.157	0.480 ± 0.004	34.79 ± 3.04
22.97	27.01	8.06	0.145	0.514 ± 0.004	37.26 ± 3.27

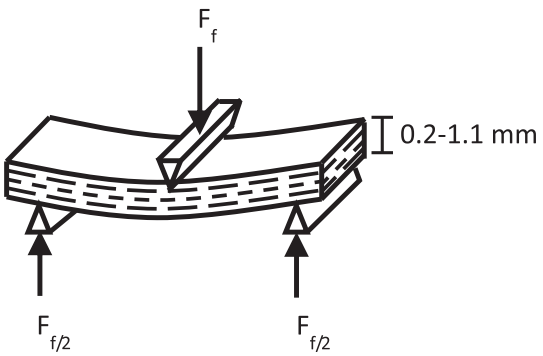

Fig. 2. Specimen configuration for dynamic mechanical testing under flexure. The dashed parallel lines show the preferred orientation of the nanotubes.

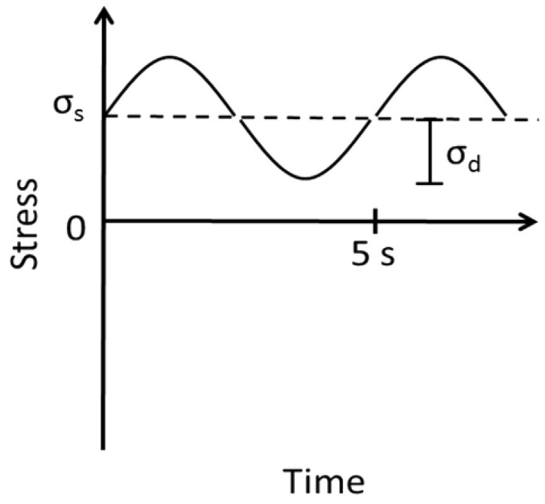

Fig. 3. Schematic illustration of the variation of the stress with time during dynamic mechanical testing under flexure. The static and dynamic stresses are σ_s and σ_d respectively.

this frequency [30–36]. Furthermore, since the loss tangent decreases with increasing frequency, the low frequency enhances the accuracy of the loss tangent measurement. The variation of stress with time is illustrated in Fig. 3.

As shown in previous work [30], the dynamic stress σ_d ranges from 1/3 to 2/3 of the corresponding static stress σ_s (Fig. 3). The deformation amplitude is kept below 10 μm in order to avoid the presence of multiple vibration modes. The flexural strain is calculated from the midspan deflection, span and specimen dimensions; the flexural stress is calculated from the load, span and specimen dimensions. The static stress ranges from 61 to 99 kPa, the dynamic stress ranges from 30 to 50 kPa, the static strain ranges from 0.031% to 0.498%, and the dynamic strain ranges from 0.005% to 0.078%. Overall, the static stress is controlled at a comparable level for all the specimens tested.

2.2.2. Instrumented indentation testing

Instrumented indentation testing in the form of nanoindentation testing under load control is conducted using a nanoindenter (MTS Systems Corporation, Model XP), equipped with a diamond Berkovich indenter tip that has a triangle-pyramidal shape and an angle of 77° between the indenter axis and each of the three side faces of the indenter tip. A high-resolution actuator is used to force the indenter into a test surface, and a high-resolution sensor is used to continuously measure the resulting penetration. The contact area under load can be inferred from the continuous load–displacement data. Thus, the residual hardness impression (the residual indent) after unloading does not have to be observed, in contrast to conventional hardness testing. The direction of indentation is that of the pressure used in forming the BNNT mat. The maximum load is 10 mN. The load resolution is 0.05 μN. The loading rate is 1.0 μN/s. In each loading cycle, the maximum load is held for 3 s before unloading; the displacement in this period is due to creep. Testing is performed at three different points on the same BNNT mat, which has thickness 0.145 ± 0.001 mm and 37.26 ± 3.27 vol.% solid (i.e., the highest solid volume fraction in Table 1).

The elastic modulus E of the specimen is determined from the reduced modulus, E_r, which is obtained by using the equation[3]

$$E_r = \frac{S\sqrt{\pi}}{2\beta\sqrt{A}}, \tag{1}$$

where S (known as the contact stiffness, i.e., the stiffness of the indenter-specimen contact) is the slope of the initial portion of the curve of load vs. displacement during unloading, β is a constant that depends only on the geometry of the indenter tip ($\beta = 1.034$ for the Berkovich tip used) and A is the projected contact area. The specimen modulus E is then obtained using the equation

$$\frac{1}{E_r} = \frac{(1-\nu^2)}{E} + \frac{(1-\nu_i^2)}{E_i}, \tag{2}$$

where E_i and ν_i are the elastic modulus and Poisson's ratio of the indenter tip ($E_i = 1141$ GPa and $\nu_i = 0.07$ for the diamond indenter tip used). The ν is the Poisson's ratio of the specimen (taken as 0.35, which is for single-walled BNNT [37]).

3. Results and discussion

3.1. Dynamic mechanical testing

Fig. 4 shows the dynamic flexural properties of BNNT mats at various solid contents (solid volume fractions). When the overall mat (including the air) is considered, the loss tangent, storage modulus and loss modulus all increase with increasing solid content. This is because the BNNTs in the mat are responsible for both the viscous and elastic characters of the mat.

Fig. 4(a) shows that the loss tangent increases from 1.01 to 3.21 with increasing solid content from 8 vol.% to 37 vol.%. This is expected, since a higher solid content is associated with more internanotube interfaces. However, the loss tangent divided by the solid content decreases from 12.6 to 8.6 with increasing solid content in the same range. The latter quantity is a better description of the material property than the former quantity, since it reflects the inherent behavior of the BNNT mat with the air contribution excluded. The decreasing trend for the loss tangent divided by the solid content means that the ease of sliding among the nanotubes decreases with increasing solid content, as expected due to the increase in the frictional force against the sliding of the BNNTs relative to one another as the BNNTs become closer to one another.

The downward trend shown in Fig. 4(a) for the loss tangent divided by the solid content is the same as that for exfoliated graphite compacts, for which the sliding is between the graphite layers in the cell wall of exfoliated graphite [30]. However, the upward trend shown in Fig. 4(a) for the loss tangent (without division by the solid content) is opposite to the downward trend for the same quantity for exfoliated graphite compacts [30]. This suggests that the ease of sliding between the graphite layers in exfoliated graphite is more sensitive to the solid content than that between the BNNTs in a BNNT mat. In other words, the sliding is hindered by an increase in the solid content more significantly for exfoliated graphite than BNNT mats. This difference between BNNT mat and exfoliated graphite is reasonable, since the graphite layers are separated from each other by just a few Angstroms [30], whereas the BNNTs in a mat are separated by much larger distances. This difference in behavior makes technology implementation less restrictive for BNNT mats than exfoliated graphite. The highest value of the loss tangent divided by the solid content is 35 for exfoliated graphite, as observed at the lowest solid content of 1 vol.% [30], whereas the highest value of this quantity is only 13 for BNNT mat, as observed at the lowest solid content of 8 vol.%. However, due to the difference in the severity of the effect of the solid content, at the same solid content of 8 vol.%,

[3] http://www.msm.cam.ac.uk/mechtest/docs/XP%20User's%20Manual.pdf,, p. 29, as viewed on Jan. 24, 2014.

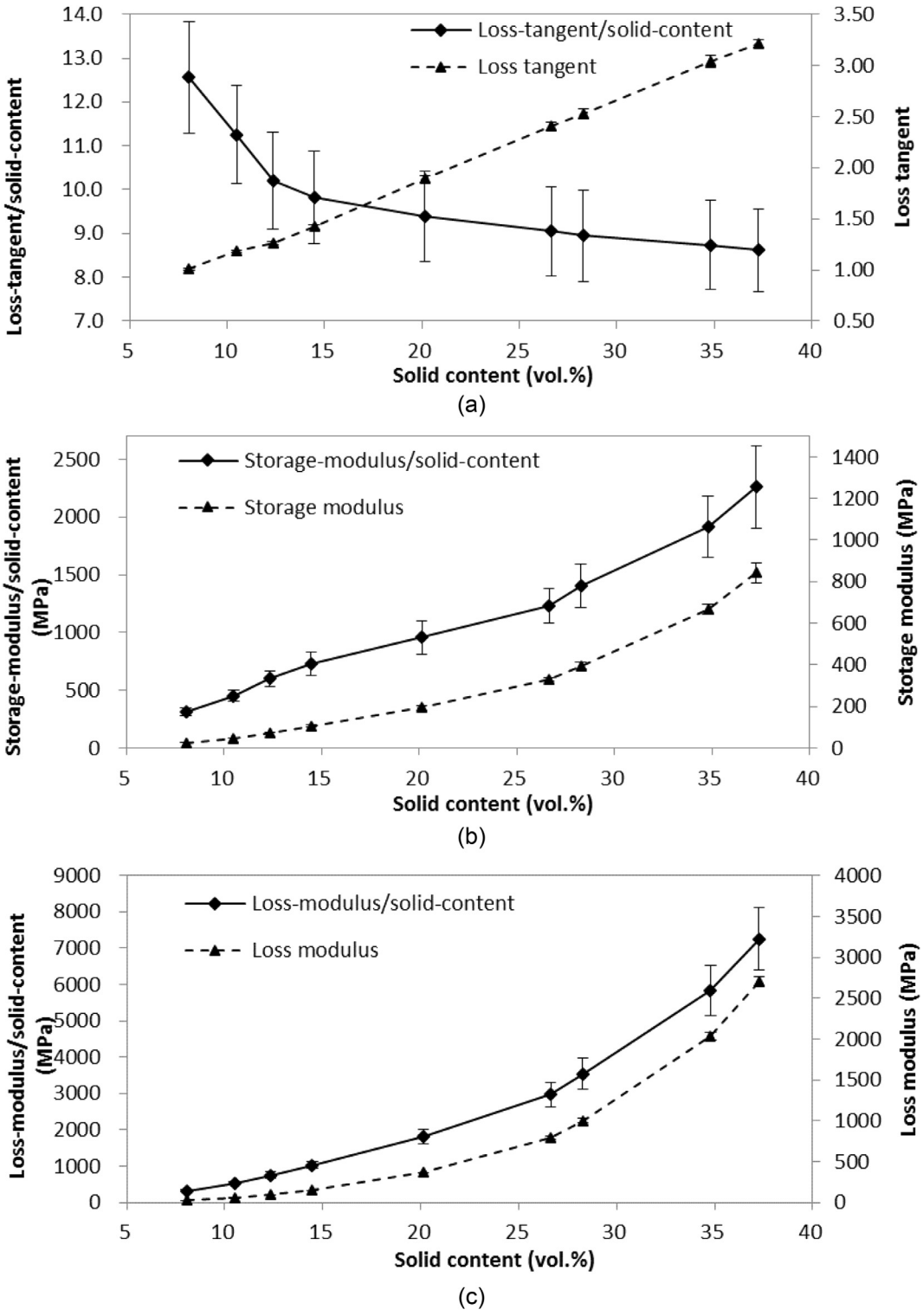

Fig. 4. Viscoelastic properties of mats at various BNNT volume fractions (i.e., various solid contents). (a) Loss tangent and loss tangent divided by the solid content. (b) Storage modulus and storage modulus divided by the solid content. (c) Loss modulus and loss modulus divided by the solid content. The errors for each of the quantities divided by the solid content are larger than those for the quantities without dividing by the solid content. The relatively large errors for the quantities divided by the solid content are mainly due to the error in the true density of the BNNTs.

this quantity is 13 for BNNT mat (Fig. 1(a)), but is only 2.0 for exfoliated graphite [30]; at the same solid content of 15 vol.%, the quantity is 10 for BNNT mat, but is only 1.0 for exfoliated graphite [30]. The higher value for BNNT mat compared to exfoliated graphite at the same solid content means that BNNT mat has a greater degree of viscous character than exfoliated graphite at the same solid content. A high degree of viscous character is valuable for vibration damping.

The loss tangent divided by the solid content describes the degree of viscous character of the BNNT mat with air excluded; the highest value is 13, which occurs at the lowest solid content. The loss tangent (without division by the solid content) describes the degree of viscous character of the BNNT mat with air included; its highest value is 3.2, which occurs at the highest solid content. The inclusion of the air lowers the degree of viscous character, as expected because the viscous character is mainly contributed by the BNNTs rather than the air.

The value of the loss tangent of rubber (nonporous), as similarly measured under flexure at the same frequency, is 0.67 [31]. This means that the BNNT mat with air excluded is much greater in the degree of viscous character than rubber. In other words, the solid part of the BNNT mat has a very strong viscous character that exceeds that of rubber, which is well-known for its viscous character. The value with air included is also greater than that of rubber. The value of the loss tangent of PTFE (polytetrafluoroethylene, nonporous), as similarly measured, is 0.19 [31]. Hence, the BNNT mat with air included is greater in the degree of viscous character than PTFE. Hence, even with air included, the degree of viscous character of the BNNT mat is greater than those of polymers that have relatively high degrees of viscous character.

Fig. 4(b) shows that the storage modulus of the BNNT mat (with the air included) increases with increasing solid content. This is expected, since BNNT is very stiff compared to air. On the other hand, the storage modulus divided by the solid content also increases with increasing solid content. This means that the stiffness of the BNNT mat (with the air excluded) also increases with increasing solid content. This suggests that the increase in proximity between adjacent BNNTs in the mat increases the stiffness of the BNNT mat (with the air excluded), due to the increasing frictional force against the sliding of the BNNTs relative to one another. The highest value of the storage modulus divided by the solid content is 2300 MPa (2.3 GPa), which is much lower than the flexural elastic modulus of 760 ± 30 GPa for an individual BNNT [37]. This relatively low modulus of the mat is expected, due to the weak link among the BNNTs in the mat.

The upward trend shown in Fig. 4(b) for the storage modulus divided by the solid content is in contrast to the essential independence of this quantity with the solid content in the case of exfoliated graphite compacts [30]. On the other hand, the upward trend shown in Fig. 4(b) for the storage modulus (without division by the solid content) is the same as that for exfoliated graphite [30]. Since the elastic stiffness relates to the ease of sliding, this means that the ease of sliding between the graphite layers in an exfoliated graphite compact is more sensitive to the solid content than that between the BNNTs in a BNNT mats. The highest value of the storage modulus divided by the solid content is 2300 MPa for BNNT mat (Fig. 4(b)), but is only 125 MPa for exfoliated graphite [30]. This adds to the attraction of BNNT mats for vibration damping. On the other hand, the value for BNNT mat is lower than the value of 9300 MPa for a cement-matrix composite containing exfoliated graphite [32].

Fig. 4(c) shows that the loss modulus of the BNNT mat, whether with the air included or not, increases with increasing solid content. This trend is the same as that of the storage modulus (Fig. 4(b)). The loss modulus divided by the solid content increases with increasing solid content in spite of the decrease of the loss tangent divided by the solid content with increasing solid content (Fig. 4(a)). This means that the loss modulus of the solid part of the BNNT mat is mostly governed by the elastic behavior rather than the viscous behavior. This is expected, since BNNT is a stiff material. On the other hand, the trend for the loss modulus of the mat (with air included) is the same as that for the storage modulus (Fig. 4(b)) as well as that for the loss tangent (Fig. 4(a)). This means that both the elastic and viscous characters contribute to the loss modulus of the mat with air included. The highest value of the loss modulus divided by the solid content is 7300 MPa. This value is comparable to the value of 7500 MPa for a cement-matrix composite containing exfoliated graphite [32] and is greater than the value of 700 MPa for short carbon fiber filled nylon, which achieves this value of the loss modulus mainly because of its high storage modulus (13 GPa), as its loss tangent is low (0.05) [38].

The upward trend shown in Fig. 4(c) for the loss modulus divided by the solid content is in contrast to the downward trend of this quantity in the case of exfoliated graphite compacts [33]. On the other hand, the upward trend shown in Fig. 4(c) for the loss modulus (without division by the solid content) is the same as that for exfoliated graphite [30]. Since the viscous stiffness relates to the ease of sliding, this means that the ease of sliding between the graphite layers in an exfoliated graphite compact is more sensitive to the solid content than that between the BNNTs in a BNNT mats. The highest value of the loss modulus divided by the solid content is 7253 MPa for BNNT mat (Fig. 4(c)), but is only 45 MPa for exfoliated graphite [30]. This adds to the attraction of BNNT mats for vibration damping.

Having high values of both the loss modulus and the loss tangent is necessary for effective vibration damping, as a high value of the loss modulus is important for mechanical energy dissipation while a high value of the loss tangent is important for an appreciable rate of decay of the vibration amplitude. For example, rubber has a high value of the loss tangent but a low value of the loss modulus [31], whereas metal-matrix composites have low values of the loss tangent but high values of the loss modulus [38]. The BNNT mat is attractive in that it has high values of both loss tangent and loss modulus. Therefore, the BNNT mat is superior to the carbon fiber filled nylon [31] and to other high-damping polymer-based and ceramic-based materials [31] for vibration damping.

3.2. Instrumented indentation testing

In spite of the absence of a binder, the BNNT mats at all solid contents investigated remain intact upon being handled by hand and is flexible. Fig. 5 shows the nanoindentation results for the BNNT mat at the highest solid content shown in Table 1. The smoothness of the load vs. displacement curve (i.e., the absence of discontinuities) indicates that the indentation mechanism involves the sliding of the nanotubes relative to one another rather than the breaking of the nanotubes. Nanotube fracture would have caused one or more discontinuities in the curve. The deformation is partly reversible upon unloading, as shown by Fig. 5. In Fig. 5, the maximum indentation depth (3400 nm = 3.4 μm) corresponds to an indent lateral size under load of 14 μm from the center of the

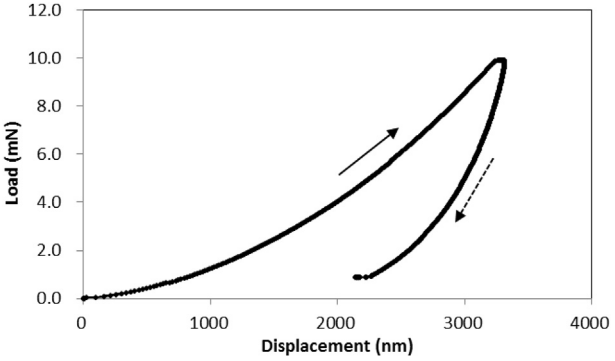

Fig. 5. Curve of load vs. displacement obtained during loading and subsequent unloading in nanoindentation testing of the BNNT mat with (37.26 ± 3.27) vol.% solid.

indent. This large indent depth and the partial reversibility of the deformation are consistent with the flexibility and viscous character of the mat.

The modulus, as determined upon unloading at the maximum load, is found to be 767 MPa for the data in Fig. 5. Based on the data obtained at three different points on the specimen, the modulus is 848 ± 132 MPa. This value, as expected, is much lower than the transverse modulus of 30 GPa for a single BNNT [37] and much lower than the longitudinal modulus of 1.2 TPa for a single BNNT [39]. Nevertheless, the value supports the mechanical integrity of the BNNT mat.

3.3. Comparison with other materials

Among all the BNNT mats studied, the overall highest values of the loss tangent (3.2), loss modulus (2.7 GPa) and storage modulus (0.83 GPa) have been achieved in the mat (overall mat, without dividing the quantity by the solid content) at the highest solid content of 37 vol.%. Table 2 shows a comparison of the dynamic mechanical properties of the BNNT mat with those of previously reported materials that are among the best for vibration damping [30,32,40–52]. These materials include carbon-based, metal-based, polymer-based and cement-based materials. The BNNT mat excels in the high value of the loss tangent, due to the interface mechanism of energy dissipation [53]. However, it is low in the storage modulus, though the value is close to that of the short jute fiber filled polymer blend [44]. Its loss modulus is high, though not the highest among the materials in Table 2. The loss tangent and loss modulus of the BNNT mat are higher than those of the interlocked CNT network (with the interlocking due to the catalyst used in CNT growth and the solid content being about 26 vol.%, based on the reported density), though the storage modulus is lower than that of the interlocked CNT network [40]. All the metal-based materials in Table 2 give low values of the loss tangent, though the storage modulus is high [50–52].

The low value of the storage modulus means that the BNNT mat is not stiff enough to be a high-performance structural material by itself. On the other hand, it may be sandwiched by stiff sheets to provide structural damping in the form of constrained-layer damping. Constrained-layer damping [54] is currently provided by the sandwiching of a polymer between stiff sheets [55,56]. The highest loss modulus in Table 2 is provided by the unidirectional carbon fiber nylon-matrix composite with an acrylic sheet interlayer [41], due to the effectiveness of the constrained-layer damping involved. Polymers are used due to their viscoelastic behavior, but they suffer from a strong dependence of their viscoelastic behavior on the temperature [57], even at temperatures in the vicinity of room temperature [41,58]. In addition, the polymer interlayer tends to decrease the modulus of the composite [58]. In contrast, ceramics such as BNNT, and carbons such as carbon nanofiber [41] have much less temperature dependence, particularly at temperatures in the vicinity of room temperature, in addition to having less tendency to decrease the elastic modulus of the composite [41].

4. Conclusions

The viscoelastic properties of BNNT mats with BNNT content ranging from 8.0 vol.% to 37 vol.% (fabricated by compaction of BNNTs with tapped density about 0.25 mg/cm^3 in the absence of a binder) have been determined under low-amplitude dynamic flexure at 0.2 Hz. The BNNT mats exhibit high degrees of viscous character (high values of the loss tangent up to 12.6 for the solid part of the mat, compared to only 0.67 for rubber), high degrees of elastic character (high values of the storage modulus up to 2.3 GPa for the solid part of the mat), and high mechanical energy dissipation ability (high values of the loss modulus up to 7.3 GPa for the solid part of the mat). These values mean that the BNNT mats have exceptionally great ability for vibration damping. It is significant that the viscous character is even stronger than that of rubber.

The loss tangent of the solid part of the mat decreases with increasing solid content, while the storage and loss moduli of the solid part increase with increasing solid content. These trends are due to the increasing difficulty for frictional sliding among the BNNTs as the solid content increases (i.e., as the BNNTs get closer to one another). As a consequence, the degree of viscous character decreases with increasing solid content, while the degree of elastic character increases. The sliding between the BNNTs in a BNNT mat becomes more difficult as the solid content increases, but the ease of sliding is less sensitive to the solid content than that between the graphite layers in an exfoliated graphite compact [33]. This difference between BNNT mat and exfoliated graphite is consistent with

Table 2
Comparison of the dynamic mechanical properties of the BNNT mat (overall, without dividing the quantities by the solid content) with those of previously reported structural materials that are among the best for vibration damping.

Material	Storage modulus (GPa)	Loss tangent	Loss modulus (GPa)
BNNT mat (37 vol.% solid) [this work]	0.83	3.2	2.7
Exfoliated graphite compact (15.5 vol.% solid) [30]	0.013	0.143	0.0019
Interlocked CNT network (~26 vol.% solid) [40]	7	0.128	0.9
Graphite cement-matrix composite [32]	9.3	0.81	7.5
Unidirectional carbon fiber nylon-matrix composite, with acrylic sheet [41]	37	0.43	16
Crossply carbon fiber epoxy-matrix composite [42]	56	0.043	2.4
Glass fiber semi-interpenetrating polymer network composite [43]	10	0.2	2
Short jute fiber filled polymer blend [44]	1	0.1	1
Short carbon fiber filled nylon [45]	13	0.05	0.7
Jute and oil palm fiber filled epoxy [46]	7	0.07	0.5
Quartz particle filled epoxy [47]	3	0.15	0.45
Hot-compacted polyethylene/polypropylene [48]	5.4	0.083	0.45
Interpenetrating polymer networks [49]	0.13	0.3	0.04
Aluminum [50]	51	0.019	1.0
Aluminum [51]	43	0.021	0.9
Nanoscale Cu–Al–Ni shape-memory alloy [52]	115	0.09	9
Zn–Al alloy [50]	74	0.021	1.5
Aluminum-matrix AlN particle composite [50]	120	0.025	3.0
Aluminum-matrix SiC particle composite [51]	45	0.024	1.1
Aluminum-matrix $ZnAl_2O_4$ coated SiC particle composite [51]	57	0.042	2.4

the much smaller distance between the graphite layers in exfoliated graphite than the separation between BNNTs in a mat. Furthermore, BNNT mat gives much higher values of both the loss modulus divided by the solid content and the storage modulus divided by the solid content than exfoliated graphite. In addition, BNNT mat has a greater degree of viscous character than exfoliated graphite at the same solid content.

When the overall mat (including the air) is considered, the loss tangent, storage modulus and loss modulus all increase with increasing solid content. This is because the BNNTs in the mat are responsible for both the viscous and elastic characters. The viscous character stems from the sliding among the BNNTs in the mat. It is consistent with a large indentation depth (14 μm) and partial reversibility of the deformation, as observed for the mat with the highest solid content of 37 vol.% with the absence of nanotube fracture.

Acknowledgment

The authors are grateful to the China Scholarship Council (Beijing, China) (201406630067) for the 12-month scholarship provided to the first author. They also thank Professor Cemalettin Basaran of University at Buffalo, State University of New York, for the use of his nanoindenter.

References

[1] Deck CP, Flowers J, McKee GSB, Vecchio K. Mechanical behavior of ultralong multiwalled carbon nanotube mats. J Appl Phys 2007;101. 023512/1–023512/9.
[2] Sugano K, Kurata M, Kawada H. Evaluation of mechanical properties of untwisted carbon nanotube yarn for application to composite materials. Carbon 2014;78:356–65.
[3] Choi Y, Choo H, Yeo H, You N, Lee DS, Ku B, et al. Chemical method for improving both electrical conductivity and mechanical properties of carbon nanotube yarn via intramolecular cross-dehydrogenative coupling. ACS Appl Mater Interfaces 2013;5:7726–30.
[4] Vargas AF, Orozco VH, Rault F, Giraud S, Devaux E, Lopez BL. Influence of fiber-like nanofillers on the rheological, mechanical, thermal and fire properties of polypropylene: an application to multifilament yarn. Compos Part A 2010;41A:1797–806.
[5] Bogdanovich AE, Bradford PD. Carbon nanotube yarn and 3-D braid composites. Part I: tensile testing and mechanical properties analysis. Compos Part A 2010;41A:230–7.
[6] Arya VP, Prasad V, Kumar PSA. Effect of magnetic field on Mott's variable-range hopping parameters in multiwalled carbon nanotube mat. J Phys Condens Matter 2012;24. 245602/1–245602/8.
[7] Saotome T, Kim H, Lashmore D, Hahn HT. Transparent conducting film: effect of mechanical stretching to optical and electrical properties of carbon nanotube mat. Bull Materi Sci 2011;34:615–22.
[8] Zhao WJ, Rochanachivapar W, Takai M. Field emission from carbon nanotube mat. J Vac Sci Technol B 2004;22:1315–8.
[9] Wang H, Wu Z, Plaseied A, Jenkins P, Simpson L, Engtrakul C, et al. Carbon nanotube modified air-cathodes for electricity production in microbial fuel cells. J Power Sources 2011;196:7465–9.
[10] Zhang Z, Dahal N, Xu K, Choi D, Yang E, Park J. Electrochemical characterization of tin quantum dots grown on a carbon nanotube mat as an anode of batteries for medical applications. Nanosci Nanotechnol Lett 2010;2:86–8.
[11] Dumitrescu I, Edgeworth JP, Unwin PR, MacPherson JV. Ultrathin carbon nanotube mat electrodes for enhanced amperometric detection. Adv Mater (Weinheim, Germany) 2009;21:3105–9.
[12] Suppiger D, Busato S, Ermanni P. Characterization of single-walled carbon nanotube mats and their performance as electromechanical actuators. Carbon 2008;46:1085–90.
[13] Zhao GL, Bagayoko D, Yang L. Unusual optical properties of aligned carbon nanotube mats in infrared energy region. J Nanosci Nanotechnol 2009;9:1603–6.
[14] Zhao G, Beeli P. Novel magnetic properties in multi-walled carbon nanotube mats: consistent with the paramagnetic Meissner effect due to ultrahigh-temperature superconductivity. Condens Matter Theor 2010;24:355–66.
[15] Zhao G, Beeli P. Novel magnetic properties in multi-walled carbon nanotube mats: consistent with the paramagnetic Meissner effect due to ultrahigh-temperature superconductivity. Int J Mod Phys B 2009;23:4285–96.
[16] Aitkaliyeva A, Shao L. The change of microstructure and thermal properties in ion irradiated carbon nanotube mats as a function of ion penetration depth. Appl Phys Lett 2013;102. 63109/1–063109/4.
[17] Varanasi C, Petry J, Brunke L, Yang BT, Lanter W, Burke J, et al. Growth of high-quality carbon nanotubes on free-standing diamond substrates. Carbon 2010;48:2442–6.
[18] Ryu J, Kim H, Lee S, Hahn HT, Lashmore D. Carbon nanotube mat as mediator-less glucose sensor electrode. J Nanosci Nanotechnol 2010;10:941–7.
[19] Padigi SK, Kunduru V, Prasad S. Multiwalled carbon nanotube-based aromatic hydrocarbon sensor using electronic dipole spectroscopy. Chem Eng Comm 2008;195:115–28.
[20] Deck CP, Ni C, Vecchio KS, Bandaru P. The mechanical response of aligned carbon nanotube mats via transmitted laser intensity measurements. In: Mater Res Soc Symp Proc 1142(Nanotubes, Nanowires, Nanobelts and Nanocoils); 2009. No pp. given, Paper #: 1142-JJ16-04.
[21] Gorintin L, Bondavalli P, Legagneux P, Chatelet M. Large-scale production of selective gas sensors based on Carbon NanoTube mats transistors. In: Mater Res Soc Symp Proc 1253(Functional materials and nanostructures for chemical and biochemical sensing); 2010. No pp. given, Paper #: 1253-K08-02.
[22] Bondavalli P. Carbon nanotubes based transistors composed of single-walled carbon nanotubes mats as gas sensors. A review. C R Phys 2010;11:389–96.
[23] Robertson J, Zhong G, Telg H, Thomsen C, Warner JH, Briggs GAD, et al. Growth and characterization of high-density mats of single-walled carbon nanotubes for interconnects. Appl Phys Lett 2008;93. 163111/1–163111/3.
[24] Han S, Chung DDL. Mechanical energy dissipation using carbon fiber polymer-matrix structural composites with filler incorporation. J Mater Sci 2012;47:2434–53.
[25] Zhi C, Bando Y, Tang C, Golberg D. Boron nitride nanotubes. Mater Sci Eng R 2010;R70:92–111.
[26] Kalay S, Yilmaz Z, Sen O, Emanet M, Kazanc E, Culha M. Synthesis of boron nitride nanotubes and their applications. Beilstein J Nanotechnol 2015;6:84–102.
[27] Zhi C, Bando Y, Tang C, Golberg D. Specific heat capacity and density of multi-walled boron nitride nanotubes by chemical vapor deposition. Solid State Comm 2011;151:183–6.
[28] Saotome T, Kim H, Lashmore D, Hahn HT. Transparent conducting film: effect of mechanical stretching to optical and electrical properties of carbon nanotube mat. Bull Mater Sci 2011;34(4):615–22.
[29] Aitkaliyeva A, Shao L. The change of microstructure and thermal properties in ion irradiated carbon nanotube mats as a function of ion penetration depth. Appl Phys Lett 2013;102(6):063109/1–063109/4.
[30] Chen P, Chung DDL. Viscoelastic behavior of the cell wall of exfoliated graphite. Carbon 2013;61:305–12.
[31] Fu W, Chung DDL. Vibration reduction ability of polymers, particularly polymethylmethacrylate and polytetrafluoroethylene. Polym Polym Compos 2001;9:423–6.
[32] Muthusamy S, Wang S, Chung DDL. Unprecedented vibration damping with high values of loss modulus and loss tangent, exhibited by cement-matrix graphite network composite. Carbon 2010;48:1457–64.
[33] Lu S, Chung DDL. Viscoelastic behavior of silica fume in the absence of a binder. ACI Mater J 2015;112:137–46.
[34] Lu S, Chung DDL. Effect of organic intercalation on the viscoelastic behavior of clay. J Mater Sci 2014;49:3189–95.
[35] Lu S, Chung DDL. Viscoelastic behavior of carbon black and its relationship with the aggregate size. Carbon 2013;60:346–55.
[36] Fu X, Chung DDL. Vibration damping admixtures for cement. Cem Concr Res 1996;26:69–75.
[37] Govind S, Bansal S. Design of mass-sensor based on resonant frequency analysis of a single walled nanotube. Int J Adv Mech Eng 2014;4(3):331–42.
[38] Chung DDL. Materials for vibration damping. J Mater Sci 2001;36:5733–8.
[39] Chopra NG, Zettl A. Measurement of the elastic modulus of a multi-wall boron nitride nanotube. Solid State Comm 1998;105(5):297–300.
[40] Liu Q, Li M, Gu Y, Wang S, Zhang Y, Li Q, et al. Interlocked CNT networks with high damping and storage modulus. Carbon 2015;86:46–53.
[41] Segiet M, Chung DDL. Discontinuous surface-treated submicron-diameter carbon filaments as an interlaminar filler in carbon fiber polymer-matrix composites for vibration reduction. Compos Inter 2000;7(4):257–76.
[42] Botelho EC, Pardini LC, Rezende MC. Damping behavior of hygrothermally Conditioned carbon fiber/epoxy laminates. J Appl Polym Sci 2007;106(5):3143–8.
[43] Khan AS, Phillips MJ, Tanner KE, Wong FS. Comparison of the visco-elastic behavior of a pre-impregnated reinforced glass fiber composite with resin-based composite. Dent Mater 2008;24:1534–8.
[44] Sarkhel G, Choudhury A. Dynamic mechanical and thermal properties of PE-EPDM based jute fiber composites. J Appl Polym Sci 2008;108:3442–53.
[45] Senthilvelan S, Gnanamoorthy R. Damping characteristics of unreinforced, glass and carbon fiber reinforced nylon 6/6 spur gears. Polym Test 2006;25:56–62.
[46] Jawaid M, Khalil HPSA, Hassan A, Dungani R, Hadiyane A. Effect of jute fibre loading on tensile and dynamic mechanical properties of oil palm epoxy composites. Compos Part B 2013;45(1):619–24.
[47] Goyanes SN, Konig PG, Marconi JD. Dynamic mechanical analysis of particulate-filled epoxy resin. J Appl Polym Sci 2003;88:883–92.
[48] Jenkins MJ, Hine PJ, Hay JN, Ward IM. Mechanical and acoustic frequency responses in flat hot-compacted polyethylene and polypropylene panels. J Appl Polym Sci 2006;99:2789–96.

[49] Babkina NV, Lipatov YS, Alekseeva TT. Damping properties of composites based on interpenetrating polymer networks formed in the presence of compatibilizing additives. Mech Compos Mater 2006;42(4):385–92.
[50] Chen P, Chung DDL. Dynamic mechanical properties of flexible graphite made from exfoliated graphite. Carbon 2012;50:283–9.
[51] Singh S, Pal K. Effect of surface modified silicon carbide particles with Al_2O_3 and nanocrystalline spinel ZnAl2O4 on mechanical and damping properties of the composite. Mater Sci Eng A 2015;644:325–36.
[52] San Juan J, Nó ML, Schuh CA. Nanoscale shape-memory alloys for ultrahigh mechanical damping. Nat Nanotechnol 2009;4:415–9.
[53] Chung DDL. Interface-derived extraordinary viscous behavior of exfoliated graphite. Carbon 2014;68:646–52.
[54] Knapp G, Oreski G, Pinter G. Method to characterize the damping behavior of thin passively constrained layer laminates using dynamic mechanical analysis (DMA) in shear mode. Polym Test 2015;42:215–24.
[55] Hujare PP, Sahasrabudhe AD. Experimental investigation of damping performance of viscoelastic material using constrained layer damping treatment. Proc Mater Sci 2014;5:726–33.
[56] Lu P, Liu XD, Ma X, Huang WB. Analysis of damping characteristics for sandwich beams with a polyurea viscoelastic layer. Adv Mater Res (Durnten-Zurich, Switzerland) 2012;374–377 (Pt. 2, Sustainable Development of Urban Environment and Building Material):764–769.
[57] Yang C, Yao D, Zou H, Mei L. Enhancing damping properties of epoxy resins using silicone macromolecule intercalated montmorillonite clay. RSC Adv 2014;4(84):44750–6.
[58] Zhang F, Guo M, Xu K, He G, Wu H, Guo S. Multilayered damping composites with damping layer/constraining layer prepared by a novel method. Compos Sci Technol 2014;101:167–72.